

Analysis of Singular Points in Fingerprints based on Topological Structure and Orientation Field

Jinwei Gu, Jie Zhou

Department of Automation, Tsinghua University, Beijing 100084, P.R.China.
gugjinwei98@mails.tsinghua.edu.cn, jzhou@tsinghua.edu.cn

Submitted to CVPR 2005

Abstract

As an important feature of fingerprints, singular points (core and delta) not only represent the local ridge pattern characteristics, but also determine the topological structure (i.e. fingerprint type) and largely influence the orientation field. In this paper, we have performed analysis for singular points in two aspects: (1) based on the topology theory in 2D manifold, we deduced the relation between cores and deltas in fingerprints. Specifically we proved that every completely captured fingerprint should have the same number of cores and deltas. We also proposed a flexible method to compute the Poincaré Index for singular points. (2) We proposed a novel algorithm for singular point detection using global orientation field. After the initial detection with the widely-used Poincaré Index method, the optimal singular points are selected to minimize the difference between the original orientation field and the model-based orientation field reconstructed from the singular points. The core-delta relation is used as a global constraint for final decision. Experimental results showed that our algorithm is rather accurate and robust. The topological properties of singular points and the detection algorithm can also be used for more general 2D oriented patterns, such as fluid flow motion, optical flow, etc.

1. Introduction

As a popular biometric feature, fingerprint is 2D oriented ridge-valley pattern captured from a finger by inked press, capacitive sensor, optical sensor, etc. Within each fingerprint, there are usually two kinds of singular points defined: *cores* and *deltas*, where the ridge orientation vanished or discontinued [1]. Fig.1 listed six typical types of fingerprints with singular points marked. As a important topological feature for fingerprints, singular points can be used for fingerprint indexing (classification for fingerprint types)[2], finger-

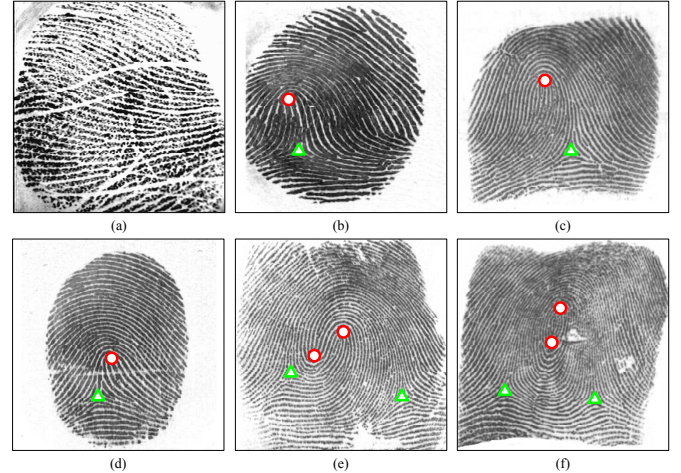


Figure 1: Various types of fingerprints with the cores (circle) and the deltas (triangle) marked: (a) Plain Arch, (b) Tented Arch, (c) Left Loop, (d) Right Loop, (e) Twin Loop, and (f) Whorl.

print alignment, orientation field modelling [3, 4], etc. They also occurs in other types of 2D oriented textures, such as fluid flow, optical flow, etc.

Many previous works were proposed for singular point detection and analysis. Shu and Jain [5] used Partial Differential Equation modelling the local patterns for various kinds of singular points in general oriented texture images. For fingerprints, the Poincaré Index is widely-used for singular points detection [2, 6, 7]. It is defined as the sum of the orientation change along a close circle around the points. Due to the noises in the real images, this local feature is not robust enough for detection. Tico et.al. [8] and Nilsson et.al.[9] used a multi-resolution approach to remove the spurious detections. Besides, there are also other approaches based on partitioning methods and heuristical rules for detection [10, 11].

Most of these works utilized the local characteristics of singular points. However, only local information

is not enough to discriminate the true singular points from those spurious detections which are caused by creases, scars, smudges, damped prints, etc. In the orientation field, these spurious detections actually have nearly the same local patterns as the true ones. More global discriminative information should be incorporated for detection. One interesting work proposed by Perona [12] is orientation diffusion, which implicitly use the global constraint of the oriented texture during the dynamic diffusion process.

In this paper, we performed analysis of singular points based on topological structures and orientation field. It can be mainly summarized as the following two folds. (1) Based on the topology theory in 2D manifold, we deduced the relation between cores and deltas in fingerprints. Specifically we proved that every *completely captured* fingerprint should have the same number of cores and deltas. We also proposed a flexible method to compute the Poincaré Index for singular points. Since the Poincaré Index is independent with the integral paths if they are homotopic, we can adaptively select the path according to the confidence of the orientation values. (2) We proposed a novel algorithm for singular points detection using the orientation field. After the initial detection with the widely-used Poincaré Index method, the optimal singular points are selected to minimize the difference between the original orientation field and the model-based orientation field reconstructed from the singular points. The core-delta relation is used as a global constraint for final decision. Experimental results showed that using both local Poincaré Index feature and the global information, our algorithm is rather accurate and robust for fingerprints with various qualities and types. The topological properties of singular points and the detection algorithm can also be used for more general 2D oriented patterns, such as fluid flow motion, optical flow, etc.

2. Topological Analysis for Fingerprint Structures

2.1. Mathematical Background

Given a continuous 2D vector field, $V(x, y) = p(x, y) + i \cdot q(x, y)$, the Poincaré Index for a path γ is defined as follows:

$$I(\gamma) = \frac{1}{2\pi} \int_{(x,y) \in \gamma} d\phi(x, y), \quad (1)$$

where $\phi(x, y) = \arg V(x, y)$ is the angle of point (x, y) on γ , $\phi \in [0, 2\pi]$. The integral is performed counter-clockwise. The Poincaré Index, also called as *winding number* in 2D topology, is an integer if the path γ is closed. By computing I along a closed circle around a point P , we can define whether P is a singular point

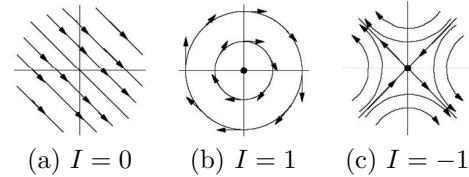


Figure 2: Three typical patterns: (a) No singularity, $I = 0$; (b) Circle, $I = 1$; (c) Saddle, $I = -1$.

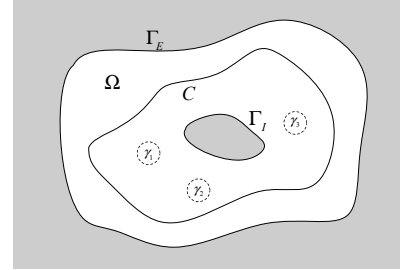


Figure 3: Region Ω with its boundary $\partial\Omega = \Gamma_E \cup \Gamma_I$. $\{\gamma_i, i = 1, 2, 3\}$ are the circles around the singular points inside Ω . C is an arbitrary closed path in Ω .

$(I \neq 0)$ or a common point ($I = 0$). In Fig.2, we listed the patterns of the common point and two typical low order singular points (circle point and saddle point). Refer [13, 14, 15] for more details.

As shown in Fig.3, suppose V is defined in the region Ω with its exterior boundary Γ_E and its interior boundary Γ_I , we denote the singular points of V inside Ω by the circles around them $\{\gamma_k | k = 1, 2, 3, \dots\}$. C is an arbitrary closed path inside Ω . There are two important properties about the Poincaré Index formulated as follows:

Property 1: The Poincaré Index of the boundary of a given region equals to the sum of the Poincaré Indexes of the singular points inside this region.

$$\sum_k I(\gamma_k) = I(\Gamma_E) - I(\Gamma_I) \quad (2)$$

Property 2: If two closed paths γ and δ are homotopic and around the same point, then

$$I(\gamma) = I(\delta) \quad (3)$$

That is, if there is no other singular points between γ and δ , then their Poincaré Indexes are the same. In Fig.3, we can easily see that $I(C) = I(\Gamma_E)$.

2.2. Analysis on Fingerprint Images

For oriented texture images, such as fingerprints and fluid flow, it is natural to establish the connection with 2D topology theory. By computing the orientation field which is defined as a matrix $O \in [0, \pi)$ representing the ridge orientation for the pixels in the image plane, we can build a vector field $V = \cos 2O + i \cdot \sin 2O$ [4,

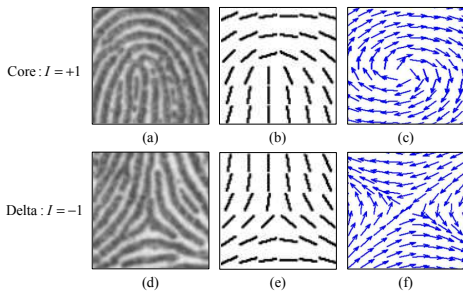


Figure 4: Singular Points in Fingerprints with the Poincaré Indexes, and their local patterns in the orientation field O and the vector field V .

[7], and apply the above definitions and properties on these images. The singular points in fingerprints are found to be consistent with the singular points defined in topology. In Fig.4, we listed typical singular points, the Poincaré Indexes, and their local patterns in the orientation field O and the vector field V .

A interesting conclusion for fingerprints can be deduced based on **Property 1**. Since fingerprints do not have interior boundary Γ_I , and only have isolated singular points (cores and deltas) with known Poincaré index (+1 for core, -1 for delta), Eqn(2) is written as

$$N_c - N_d = I(\Gamma_E), \quad (4)$$

where N_c is the number of the cores, N_d is the number of the deltas, and Γ_E is the exterior boundary of the fingerprint.

As shown in Fig.5(c), if a fingerprint is captured completely, it can be assumed that the *left, right, bottom, and top* boundaries are nearly *horizontal*. Although different type fingerprints can vary inside, this assumption still hold for their boundaries. For the path Γ_E consisting of this kind of boundaries, $I(\Gamma_E) = 0$, and then $N_c = N_d$. Therefore, we concluded that for each *completely captured* fingerprint, there are the same numbers of cores and deltas. Although there are previous works which implicitly pointed out cores and deltas could be cancelled by each other like positive and negative charges [2, 4], we theoretically proved that cores and deltas should be appeared in couples. Two views of a real thumb are shown as an example in Fig.5(a)(b) with the cores and the deltas marked. Eqn(2)-(4) can also be applied on other oriented patterns. For example, for human hair, by assuming the hair is outwards at the boundary, the sum of the Poincaré indexes is 1, so there must be at least one hair vortex.

As for **Property 2**, we know that the Poincaré Index can be computed along any closed path as long as it is homotopic with the closed circle around the point (i.e., not include any new singular point). This allows

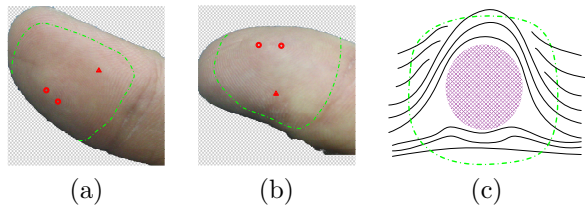


Figure 5: Left (a) and right (b) views of a real thumb with singular points and boundary marked. (c) shows the boundary of a complete fingerprint abstraction.

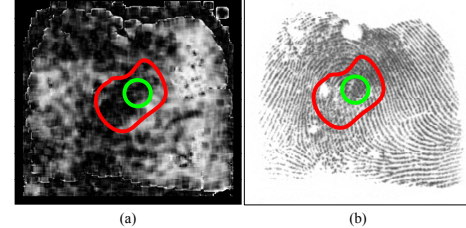


Figure 6: Adaptively choose the integral path for the Poincaré Index Computation based on the homotopic property. (a) The confidence of the orientation field [16]. (b) The selected optimal path (red) where the confidence is high and the conventional circle (green). The selected path can give the correct Poincaré Index ($I = 1$) while the circle is not ($I = 0$).

us to adaptively choose the integral path, for example, the path where the orientation confidence is high. An example is shown in Fig.6.

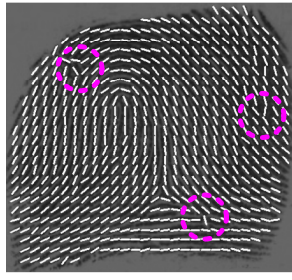
2.3. Practical Considerations

In real applications, many fingerprint images captured by optical or capacitive sensors are not complete. Usually they will lose one or two deltas. In this case, the number of cores is not necessarily equal to the number of deltas. Nevertheless, Eqn(4) still presents us a global topological constraint for singular points. Suppose the effective region of the fingerprints is Ω , by computing $I(\partial\Omega)$, we can know that only finite combinations of the singular points are valid. In Table 1, we listed most of the possible combinations of singular points for fingerprints with the Poincaré Index and the possible types (PA-plain arch, TA-tented arch, LL-left loop, RL-right loop, TL-twin loop).

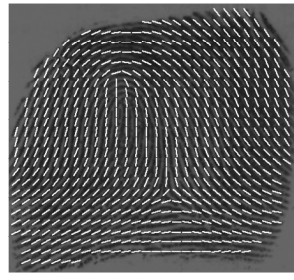
Table 1: Frequent combinations of singular points

$I(\partial\Omega)$	Core	Delta	Possible Types
0	0	0	PA
	1	1	LL, RL, TA
	2	2	TL, Whorl
1	1	0	LL, RL, TA
	2	1	TL, Whorl
2	2	0	TL, Whorl

In practice, the orientation field O directly extracted



(a)



(b)

Figure 7: Computation of the orientation field in practice: (a) hierarchical gradient-based method [17], (b) polynomial model based method [18].

from the images will contain lots of noises due to creases, scars, blurring, etc. As shown in Fig.7(a), the original orientation field, O , is computed using the state-of-the-art hierarchical gradient-based method [17]. Although it works well in most of the effective region, there are still some noises in the marked areas, which however will influence the computation of $I(\partial\Omega)$. To smooth out this kind of noises, we adopted the polynomial model based method proposed by Zhou and Gu in [18]. They used two bivariate polynomials, $P(x, y) = \sum_{i,j} p_{ij} x^i y^j$ and $Q(x, y) = \sum_{i,j} q_{ij} x^i y^j$, to approximate $\cos 2O$ and $\sin 2O$, respectively. The parameters, $\{p_{ij}, q_{ij}\}$, can be estimated with Least Square method linearly. After this approximation, the smoothed orientation field can be reconstructed as:

$$O(x, y) = \frac{1}{2} \arctan \frac{\sum_{i,j} q_{ij} x^i y^j}{\sum_{i,j} p_{ij} x^i y^j}. \quad (5)$$

Fig.7(b) shows the orientation field after smoothing. Although the polynomial-based reconstruction is not good enough at the regions near the singular points in the center of Ω , it can well model the orientation field near the boundary and effectively remove the noises, and thus keep the global topological property invariant. This is just what we want to robustly compute $I(\partial\Omega)$. In Fig.8, we listed two fingerprints along with the corresponding $I(\partial\Omega)$ and the singular points. The results verified our conclusion about the topological constraint about the singular points.

3. Singular Point Detection with Global Information

In this section, we proposed a novel algorithm for singular point detection using the global orientation field. As pointed out, only local features are not enough to discriminate the true singular points from those spurious detections, which actually have nearly the same

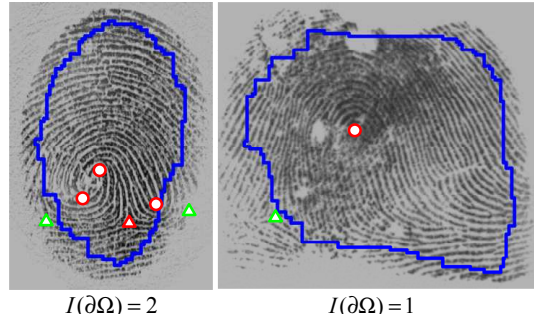


Figure 8: Two examples for the topological analysis of fingerprints. The blue curves are the boundary of the effective region. Circles are cores and triangles are deltas. The detected singular points are marked as red, while the singular points outside Ω are marked with green.

local characteristics as the true ones. This motivates us to incorporate more global discriminative information for detection.

As known, singular points almost determine the global orientation field of fingerprints. In fact, there are several orientation field models related to singular points [3, 4, 19]. Our basic idea is to select the final optimal singular points by minimizing the difference between the original orientation field and the model-based orientation field reconstructed from the singular points. Specifically, each singular point detection is denoted by a triple, (x, y, t) , with its positions and type (core/delta). All singular point candidates are in the set $S = \{(x_i, y_i, t_i)\}_{i=1}^M$. The true singular points, s , is a subset of S . Denote the original orientation field with O_0 , the reconstructed orientation field with $O(\Theta, s)$ where Θ is the model's parameter. The optimal singular points can be selected as:

$$s^* = \arg \min_{s \subseteq S} \|O_0 - O(\Theta, s)\|, \quad (6)$$

where the difference function, $\|\cdot\|$, is defined later.

Besides, the core-delta relation deduced in the above section can also be used as a global constraint for the optimal singular points selection. By computing the global Poincaré Index $I(\partial\Omega)$, we can easily remove some invalid combinations of singular points based on Table.1 and speed up the algorithm.

Finally, we would like to emphasize that the widely-used Poincaré Index method will not miss the true singular points as long as the process scale is low enough (i.e. small circle for computing), although it has lots of spurious detections. Actually this local method can detect the precise positions of the true singular points. This property guarantees our proposed method's robust and accurate performance after removing spurious detections. The flowchart of the whole detection algo-

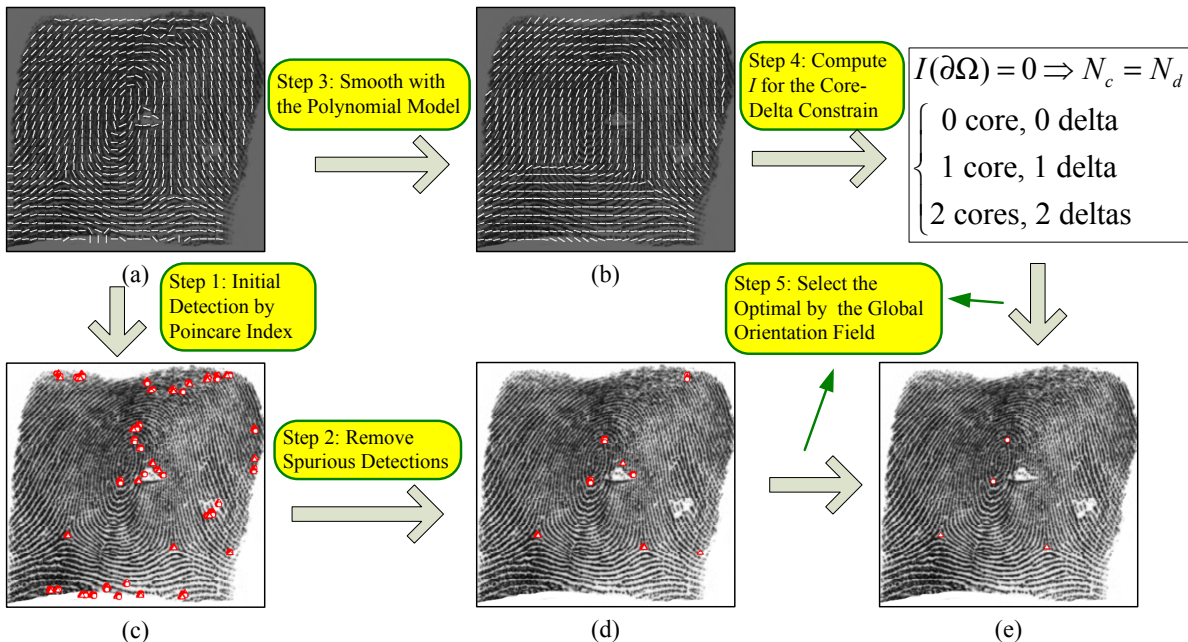


Figure 9: Flowchart of our proposed detection method

rithm is shown in Fig.9. The details will be explained as follows.

3.1. Orientation Field Computation

The original orientation field, O_0 , is computed by the hierarchical gradient-based method [17]. As for the model-based reconstructed orientation field, $O(\Theta, s)$, we choose the *Zero-Pole* model proposed by Sherlock and Monro in [3], considering both the model accuracy and the computational efficiency. This model is based on the singular points, s , which takes the cores as zeros and the deltas as poles in the complex plane. It can be formulated as:

$$O(x, y; \phi, s) = \frac{1}{2} \arg \left(e^{i\phi} \cdot \frac{\prod_i (z - z_{c_i})}{\prod_j (z - z_{d_j})} \right), \quad (7)$$

where $z = x + iy$, z_{c_i} is the i -th core, z_{d_j} is the j -th delta, $\phi \in [-\pi, \pi]$ is a *background angle* to be decided. However, how to estimate ϕ is not mentioned in previous works till now. In this paper, we propose to estimate the background angle ϕ under the Least Square meaning. Suppose $O_1(x, y)$ is $O(x, y; \phi, s)$ when $\phi = 0$, the optimal ϕ is estimated by:

$$\phi^* = \arg \min_{\phi} J(\phi), \quad (8)$$

where

$$J(\phi) = \sum_{\Omega} (\sin(2O_1 + \phi) - \sin 2O_0)^2 + (\cos(2O_1 + \phi) - \cos 2O_0)^2.$$

The difference function in Eqn(6), $\|O_0 - O(\Theta, s)\|$, is defined as $J(\phi^*)$ above.

3.2. Spurious Detections Removal

As shown in Fig.9, after the first step with the Poincaré Index, lots of spurious points are detected. In this part, we proposed to remove them with a novel feature, D , which is a vector consisting the Differences of the ORIENTATION values along a Circle (DORIC) around the point. For a given point P , we uniformly sampled a set of points, $\{T_1, T_2, \dots, T_L = T_1\}$, along a circle around it in anticlockwise direction. The feature can be formulated as:

$$D(P) = [\delta O_1, \dots, \delta O_i, \dots, \delta O_L], \quad (9)$$

where O_i is the value of the orientation field O at point T_i , $\delta O_i = O_{mod(i+1, L)} - O_i$. Fig.10 showed three typical texture patterns and their DORIC feature plotted as curves. Since the orientation field O is defined in $[0, \pi]$ instead of $[0, 2\pi]$, there will be a pulse for singular points (positive pulse for core, negative pulse for delta).

This feature has strong relations with the Poincaré Index defined in Eqn(1). Given a function $f(x)$ which equals to x when $|x| < \pi/2$, $\pi - x$ when $x > \pi/2$, and $\pi + x$ when $x < -\pi/2$, it can be proved that $I = \frac{1}{\pi} \sum_{i=1}^L f(\delta O_i)$. Although it is still a local feature, DORIC contains more discriminative information than the Poincaré Index. Fig.11 showed two examples from

a poor-quality fingerprint, which are falsely detected as core and delta by the Poincaré Index method but have very different DORIC features compared with true ones shown in Fig.10.

For each point with non-zero Poincaré Index, we compute its DORIC feature. If there is exactly one pulse with the height nearly up to π , it is a valid candidate singular point; otherwise it will be removed from the candidate set S . In practice, multiple DORIC features are computed along a set of circles at different scales around the point P . Based on the votes from these multiple-scale DORIC features, we made the decision whether it should be removed from the candidate set S . Extensive experimental results proved that this feature can effectively remove spurious detections and can be computed very fast (see Fig.9 for example).

4. Experimental Results

The fingerprint database used in this paper consists of three parts. The first part contains 800 fingerprint images captured from 100 non-habituuated cooperative subjects with a Digital Persona optical sensor, whose size is 512×320 (pixels). The second part is a sample database from NIST Special Database 14 [20] that contains 40 inked fingerprint images. The image size is 480×512 (pixels). The third part is from FVC2000 database (DB1, DB2, and DB3) [21] with $80 \times 3 = 240$ images captured by capacitive sensor and optical sensor. Thus there are total 1080 fingerprints in our database including various qualities and types. The singular points of these fingerprints are manually labelled by experts as the ground truth beforehand.

Firstly, we carried experiments to verify the topological properties presented in Section 2 for fingerprints. We computed the Poincaré Index, $I(\partial\Omega)$ and counted the numbers of cores and deltas inside and outside the effective region Ω . The results on all the fingerprints in the database verified our conclusions that: (1) the cores and the deltas should be appeared in couples, and (2) the two topological properties can be well applied on fingerprint images. Fig.8 showed two examples which are the accidental type or poor-quality for illustrations.

Secondly, we performed singular points detection according to the algorithm shown in Fig.9. The implementation details are summarized as follows. The effective region Ω is extracted by computing the mean and the variance of the intensity value on each block and doing simple binarization (an "effective" block should have the mean in [20, 220] and the variance greater than 6 in our study). A post process including dilation and erosion is made to remove some isolate points and to fill large holes. For the Poincaré Index method, we choose a circle with the radius as 2 pixels for initial de-

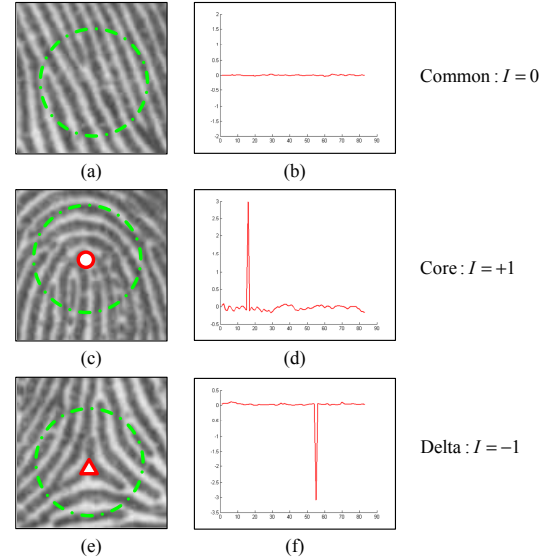


Figure 10: Typical texture patterns and their DORIC features plotted as curves. There is a positive pulse for the core and a negative pulse for the delta. The height of the pulses are nearly up to π .

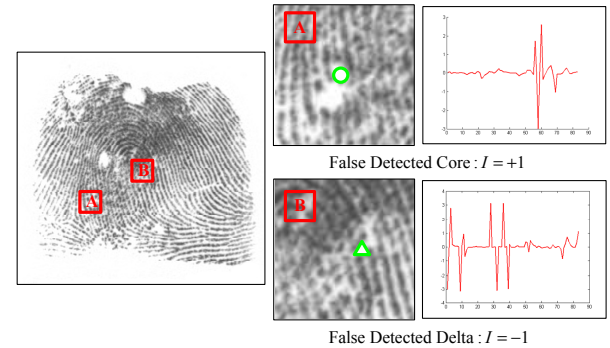


Figure 11: Typical false detected examples by the Poincaré Index, and their DORIC features plotted as curves. The features are different with those of the true singular points.

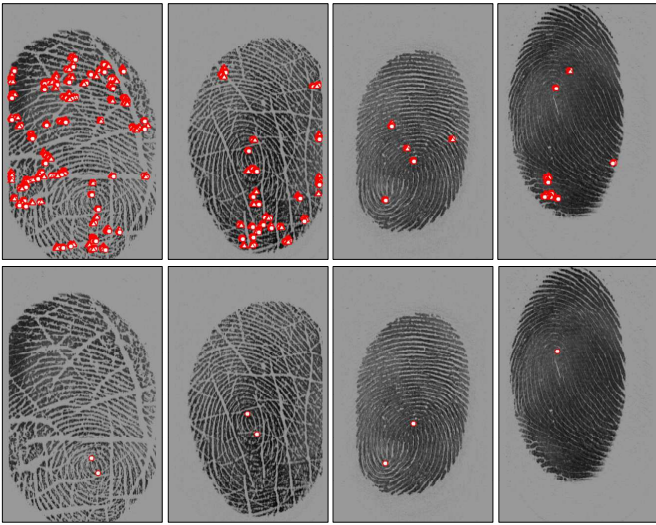


Figure 12: Singular points detection results on various types of fingerprints. The first row are based on the widely-used Poincaré Index method, and the second row are based on our proposed method. These fingerprints cover most of the difficult situations for singular point detection: dryness, damped or blurred prints, and serious creases or scars.

tection. The order of the polynomials is set as 4 in the orientation-field-smoothing step. For DORIC feature, we compute it at three scales and the radiiuses of the circles are 5,7,9 pixels.

In Fig.12, we presented the detection results on some typical fingerprints which cover almost all the difficulties for singular point detection such as creases, scars, smudges, dryness, damped or blurred prints, etc. The first row showed the detected results with the widely-used Poincaré Index method. The second row showed the results of our proposed method. Although we did not implement all of the previous methods using various heuristic rules or multiple resolution, we would like to emphasize that without global constrains, it is very hard to remove the spurious detections on these fingerprints. With our method, the singular points are robustly detected and the positions are rather accurate. More results are shown in Fig.13.

Table 2: Detection results

	Correct	Missing	False Detect
Percentage	80.6%	14.6%	4.8%

To get the statistical performance of this algorithm, we made the following definitions for each detection result. For a given fingerprint, all of the detected singular points are denoted by $s = \{(x, y, t)\}$, all of its ground truth singular points are denoted by $s_0 = \{(x_0, y_0, t_0)\}$. Any two singular points are said to be *equivalent* if and



Figure 13: More singular points detection results by our algorithm.

only if $t = t_0$ and $|x - x_0| < 5$ (pixels), $|y - y_0| < 5$ (pixels). So, if all of the detections in s are correct detections and all of the ground truth points in s_0 are correctly detected, then the singular points of the fingerprint are said to be *correctly* extracted. If all of the detections in s are correct detections but at least one of the ground truth points in s_0 is not correctly detected, then it is said that the algorithm *misses* some singular points. Otherwise, it is said the singular points are *false*ly detected. With these definitions, we presented the percentage for *correct*, *missing*, and *false detect* in Table 2. We found that for most of the *missing* cases, it is usually that one or two deltas are not detected. Since the cores (if available) can be correctly detected, the detection results are still good for applications. Based on these results (especially the low false detect rate), our algorithm shows satisfactory performance for real applications.

Another advantage of our method is its real-time processing speed. Both the polynomial-based smoothing and the selection with the global orientation field can be done linearly by Least Square Method. The Zero-Pole model-based reconstruction won't take much time. And the topological constraint and DORIC feature will also effectively remove lots of spurious detections. It is currently implemented with Matlab and C on a AMD 2200Hz 512M PC computer without optimization. The average processing time for each fingerprint is around 0.10 sec.

5. Conclusions and Discussions

To sum up, we focus on singular points of fingerprints in this paper. Our contributions lie in two aspects. (1) We analyzed the topological relations of different types

of singular points in 2D oriented textures. For completely captured fingerprints, we concluded that cores and deltas should be appeared in couples. It is also a global constraint for fingerprints' singular points in real applications. Both the topological properties can be applied on more general patterns. (2) We proposed a novel algorithm for singular points detection using the global orientation field. The optimal singular points can be selected by minimizing the difference between the original orientation field and the model-based orientation field reconstructed from the singular points. We also proposed a new feature DORIC other than the Poincaré Index, which can effectively remove the spurious detections. Results show that our analysis and the detection algorithm are effective for singular points.

Topological analysis on manifolds is a very interesting topic. In this paper we only discuss two basic properties in 2D vector field. How to apply them as a global constraint for singular points in 3D or higher dimensional manifold? How to apply more topology properties such as the Poincaré -Hopf theorem for singular points detections or shape analysis? These open problems will be investigated in our further research.

References

- [1] D. Maltoni, D. Maio, A. K. Jain, and S. Prabhaker. *Handbook of Fingerprint Recognition*. Springer-Verlag New York, Inc., 2003.
- [2] K. Karu and A. K. Jain. Fingerprint classification. *Pattern Recognition*, 17(3):389–404, 1996.
- [3] B. Sherlock and D. Monro. A model for interpreting fingerprint topology. *Pattern Recognition*, 26(7):1047–1055, 1993.
- [4] J. Gu and J. Zhou. A novel model for orientation field of fingerprints. *IEEE Int. Conf. on Computer Vision and Pattern Recognition*, 2:493–498, June 2003.
- [5] Chiao-Fe Shu and Ramesh C. Jain. Vector field analysis for oriented patterns. *IEEE Trans. on Pattern Analysis and Machine Intelligence*, 16(9):946–950, September 1994.
- [6] A. K. Jain, S. Prabhakar, and L. Hong. A multichannel approach to fingerprint classification. *IEEE Trans. on Pattern Analysis and Machine Intelligence*, 21(4):348–359, 1999.
- [7] A. M. Bazen. Systematic methods for the computation of the directional fields and singular points of fingerprints. *IEEE Trans. on Pattern Analysis and Machine Intelligence*, 24(7):905–919, July 2002.
- [8] M. Tico and P. Kuosmanen. A multiresolution method for singular points detection in fingerprint images. *IEEE Int. Conf. on ISCAS*, 4:183–186, July 1999.
- [9] K. Nilsson and J. Bigun. Complex filters applied to fingerprint images detecting prominent symmetry points used for alignment. *in Proc. Workshop on Biometric Authentification (in ECCV 2002)*, pages 39–47, 2002.
- [10] R. Cappelli, A. Lumini, D. Maio, and D. Maltoni. Fingerprint classification by directional image partitioning. *IEEE Trans. on Pattern Analysis and Machine Intelligence*, 21(5):402–421, May 1999.
- [11] P. Ramo, M. Tico, V. Onnia, and J. Saarinen. Optimized singular point detection algorithm for fingerprint images. *IEEE Int. Conf. on ICIP*, 3(3):242–245, October 2001.
- [12] P. Perona. Orientation diffusions. *IEEE Trans. on Image Processing*, 7(3):457–467, 1998.
- [13] William Fulton. *Algebraic Topology: A First Course*. Springer-Verlag New York Inc., 1995.
- [14] Gerik Scheuermann. *Topological Vector Field Visualization with Clifford Algebra*. PhD thesis, January 1999.
- [15] G. Scheuermann, H. Krüger, M. Menzel, and A. P. Rockwood. Visualizing nonlinear vector field topology. *IEEE Trans. on Visualization and Computer Graphics*, 4(2):109–116, 1998.
- [16] M. Kass and A. Witkin. Analyzing oriented pattern. *Computer Vision, Graphics and Image Processing*, 37:362–397, 1987.
- [17] A. K. Jain and L. Hong. On-line fingerprint verification. *IEEE Trans. on Pattern Analysis and Machine Intelligence*, 19(4):302–314, April 1997.
- [18] J. Zhou and J. Gu. A model-based method for the computation of fingerprints' orientation field. *IEEE Trans. on Image Processing*, 13(6):821–835, June 2004.
- [19] J. Zhou and J. Gu. Modeling orientation fields of fingerprints with rational complex functions. *Pattern Recognition*, 37(2):389–391, February 2004.
- [20] Sample of nist special database 14: Nist mated fingerprint card pairs (mfcp2). Available at <http://www.nist.gov/srd/nistsd14.htm>.
- [21] D. Maio, D. Maltoni, R. Cappelli, J. L. Wayman, and A. K. Jain. Fvc2000: Fingerprint verification competition. *IEEE Trans. on Pattern Analysis and Machine Intelligence*, 24(3):402–412, March 2002.